International Journal of Nanoelectronics and Materials
IJNeaM
ISSN 1985-5761 | E-ISSN 2232-1535

DFT modeling of new composite based on PANI/PVK functionalized With single-walled carbon nanotubes for optoelectronic applications

Boubaker Zaidi [a,b,*]

[a]*Department of Physics, College of Science and Humanities, Shaqra University, Dawadmi 11911, Saudi Arabia.*
Laboratoire de Synthèse Asymétrique et Ingénierie Moléculaire de Matériaux Organiques Pour L'électronique Organique LR 18ES19,
[b]*Department of Physics, Faculty of Science, University of Monastir, Monastir 5019, Tunisia.*
∗Corresponding author. e-mail: boubaker@su.edu.sa

Received 20 February 2023, Revised 2 May 2023, Accepted 31 August 2023

ABSTRACT

We present a comparative experimental and theoretical study of the vibrational, optical, and electronic properties of polyaniline at both emeraladine leuco-emeraldine forms and PVK. Our objective is first to select the appropriate form of PANI to be linked with PVK to form a hybrid polymer matrix. Then, on the basis of quantum chemical calculations, we present a theoretical study of a hybrid composite PANI/PVK functionalized with lower radius (5, 5) chiral single-walled carbon nanotubes (SWCNTs). The relationship structure-properties of the resulting nano-composite are proved based on the conformational and optical study made from Density functional theory (DFT) and time-dependent density functional theory (TD-DFT) using B3LYP method with 6-31-G(d) basis set. First, it has been demonstrated that the resulting interaction between PANI and PVK leads to more advantageous properties, such as good optical absorption compatibility with the solar emission spectrum. It has also been found that after the incorporation of SWCNTs into the matrix of PANI/PVK hybrid polymer, a good organization of SWCNTs via π-staking interaction is imposed by polyaniline sequences. However, PVK moieties are grafted on the sidewalls of SWCNTs. Finally, the electronic structure of the resulting hybrid nano-composite PANI/PVK/SWCNTs was carried out with the use of different electrodes on both sides.

Keywords: *Carbon nanotubes, Charge Transfer, DFT, Electronic structure, Nano-composite*

1. Introduction

Renewable energy sources are of great importance for both environmental and economic points of view [1,2]. In order to reach better SWCNTs dispersion in the polymeric matrix, a lower SWCNTs weight concentration is often added. This weak concentration greatly leads to improving the photovoltaic power conversion efficiencies [10] due to the charge transfer occurring at the hetero-nano-junctions. Moreover, SWCNTs are known by a good factor form (ratio: Length/diameter ≈ 500) and higher hole and electron mobilities, allowing them the properties of a good transporting layer [11]. On the other hand, as recently published, the combination of polymers can drive new exceptional properties due to their complementarity [12]. However, the hybrid material resulting from both PVK and PANI has not yet been studied in pristine and nanostructured states. Starting from this point of view, we present in this paper a combined experimental and theoretical study based on the density functional theory (DFT), the resulting hybrid material (PANI/PVK), and its functionalization with lower radius (5,5) Chiral SWCNTs. Firstly, our aim is to demonstrate the molecular structure of the resulting hybrid polymer based on both PANI and PVK sequences and to justify the corresponding functionalization process with SWCNTs. Secondly, we give a description of the properties of the resulting Bulk Hetero-nano-junction solar cell.

In this context, to reach a better trade-off, the photovoltaic conversion field needs new lower cost and easier processing methods [3]. For three decades, polymeric materials have been largely classified as concurrent materials for silicon to be used as active layers due to their excellent properties, such as flexibility and easier thin film elaboration [4]. Among these materials, polyaniline (PANI) and poly(N-vinyl carbazole) PVK are largely studied for their excellent properties [4,5,6], especially the electron excess related to the nitrogen atom present in both materials. In our previous works [6, 7, 8,9], we demonstrated that these materials could be functionalized with lower concentration single-walled carbon nanotubes (SWCNTs). For both PANI and PVK, the exchange process with SWCNTs is governed by a covalent functionalization and leads to a charge transfer from the polymeric matrix to the SWCNTs. This transfer at the nanometer scale gives rise to the improvement of photovoltaic properties, especially the compatibility with the solar spectrum in the absorption process and the accordance between the diffusion length and the nano-junction size.

2. MATERIALS AND METHOD

Both materials (PANI, PVK) were purchased from Sigma-Aldrich. The PANI powder is characterized by an average molecular weight: Mn > 15,000, a purity of 99.99%, a refractive index of 1.85, a melting point >570 K, and a density of 1.36 g/ml at 300 K. The PVK polymer has the average molecular weight Mw = 1,100,000, Mn varying from 25,000 to 50,000, a melting point of 572 K and a density of 1.2 g/ml.

FTIR measurements are taken from KBr pellets painted with the organic compound under study using a Bruker Vertox 80 V interferometer with a resolution of 4 cm−1.

For optical absorption measurements, the obtained composites or the PANI solution, at either annealed or not annealed states, were deposited at room temperature with nearly uniform thickness on silica substrates already cleaned with deionized water and ethanol in an ultrasonic bath. Then, all samples thus obtained were introduced into a Pyrex tube and then sealed and heated under vacuum at the temperatures of 393 K. The optical absorption spectra are recorded using UV1800 spectrophotometer working in the absorption mode with the wavelength varying from 200 nm (6.2 eV) to 2,000 nm (0.62 eV).

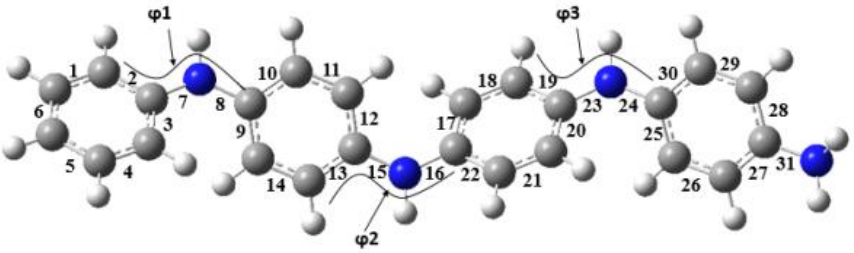

(a)

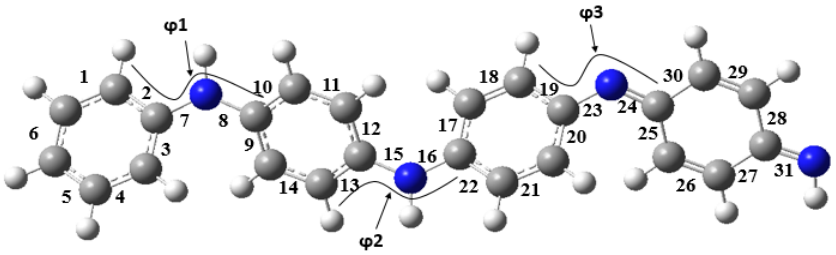

(b)

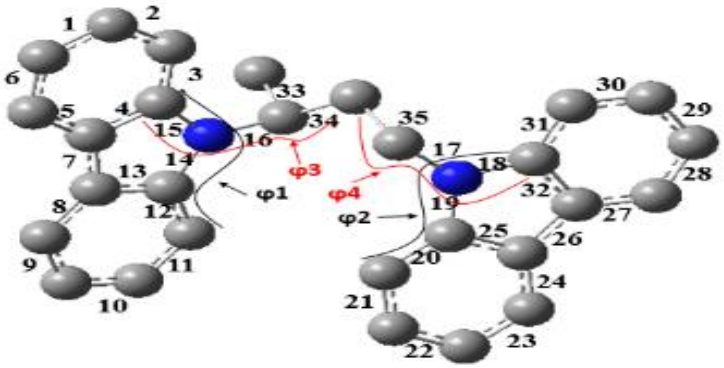

(c)

Figure 1 Geometrical structure of (a) Leucoemeraldine and (b) Emeraldine base and (c) PVK.

For computational details, all the molecular structures of all the materials used in this study, including composites PANI/PVK and PANI/PVK/SWCNTs (Figure 1), are predicted by the density functional theory (DFT) and the time-dependent density functional theory (TD-DFT), using B3LYP method with 6-31-G(d) basis set. For the SWCNTs structure, the calculations consist of optimizing the geometry of SWCNTs with chirality (n,m)=(5.5), diameter Φ= 0.71 nm, and length L = 100 nm (150 atoms). The two polymers that constitute the subject of this study are saturated at their ends by hydrogen bonds, which can avoid covalent functionalization on the surfaces of SWCNTs and also favor a plane configuration (π-stacking). To reduce the calculation time, the composite structure PANI-EB/PVK/SWCNTs, which is considered a longer molecule, was first carried out using the semi-empirical PM3 method. The resulting configuration was re-optimized using the DFT/B3LYP/6-31G (d). This method has been considered a preferred and effective approach that takes into account the majority of interactions that govern the structure of composites. Otherwise, the electronic and optical transition in the absorption process of all molecular configurations has been calculated using the SWIZAR program..

3. RESULTS AND DISCUSSION

In order to differentiate between the two forms of PANI (leucoemeraldine and emeraldine base), especially the imine and amine functions, we present in Figure 2 the results of the optimization at their ground states, including the interatomic bonds, the dihedral angles, and stabilizing energy.

Interatomic distances as a function of the bond number for the two forms of PANI and those of PVK modeling structure are presented in Figure 1. Both forms of PANI present nearly identical interatomic distances in the common neutral fragment, varying from 1.391 Å to 1.407 Å (a maximum for the C-N bonds). However, a noticeable change in the bond lengths associated with the quinoide sequence, starting from bond number 23 (between 1.294 Å and 1.469 Å), is observed. This demonstrates that the quinoid form is the signature of a strong electron delocalization and, consequently, a more extensive conjugation [13]. On the other hand, as shown in Figure 1 and Table 1, the theoretical dihedral angles obtained between the different rings of PANI in both forms confirm non-planar geometries. It is noted that the highest values correspond to the leucoemeraldine, suggesting that the geometry of the emeraldine base is less deformed than that of leucoemeraldine. As electron delocalization is restricted to the conjugated fragments, which favors a planar geometry, it can be concluded that the emeraldine base form has better transport properties than the leucoemeraldine form [14,15].

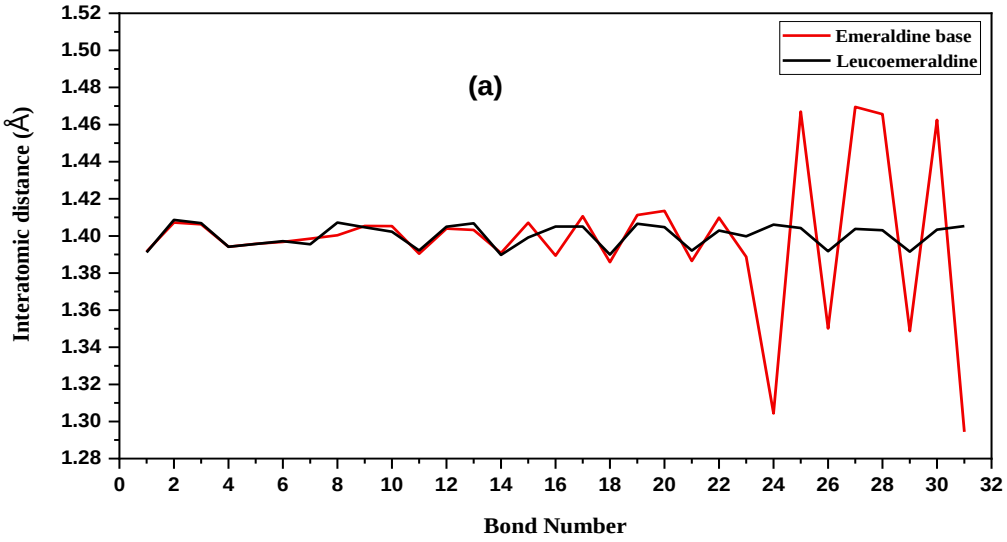

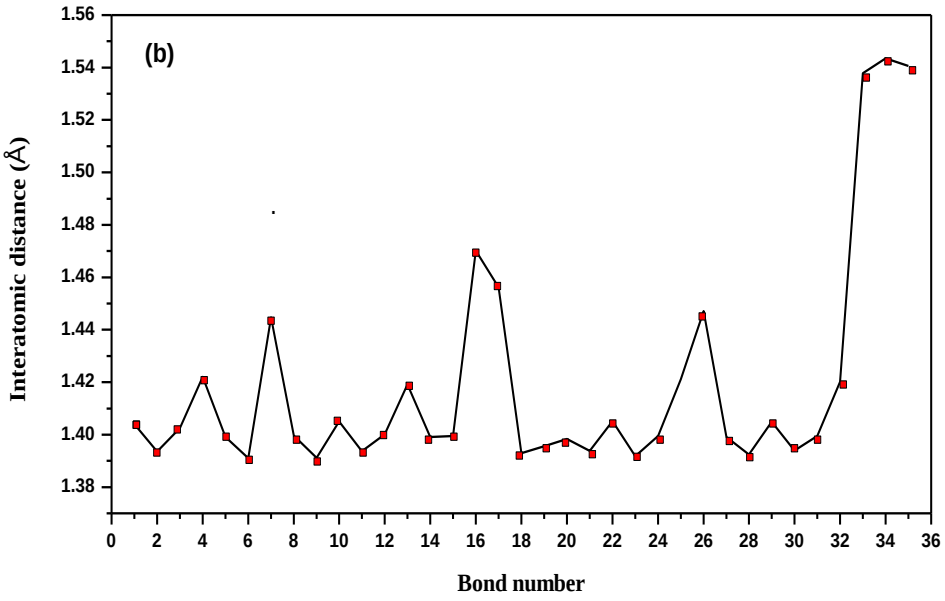

Figure 2. Interatomic distance of (a) PANI and (b) of PVK.

Table 1 Ring torsion angle of Polyaniline and PVK.

	φ1 (°)	φ2 (°)	φ3 (°)	φ4 (°)
Emeraldine base	43.191	-43.658	41.742	--------
Leucomeraldine	44.812	-44.670	46.033	--------
PVK	0.13	-0.06	60.83	71.07

The analysis of the variations of interatomic distances of PVK (Figure 1, with stabilizing energy Estab = -1190.989Ha, as a function of the bond number demonstrates that most changes are observed on neighboring atoms of the nitrogen, as reported by P. R. Sundararajan [16]. Contrary to the polyaniline, the presence of nitrogen atoms in the heterocycle gave the molecule a planar geometry due to the self-induced columbic interactions [16]. The values of the angles φ1 and φ2 between the carbazole benzenoid rings are nearly 180 °, indicating their planar geometry configuration. The aliphatic sequences (CH3 - CH - CH - CH2) undergo the dihedral angles φ3 and φ4 values , which tend towards the perpendicular direction (90 °). As the electron delocalization favors the total flat geometry [14], carbazole benzenoid rings are the only fragments allowing this delocalization [17].

In order to elucidate the difference between the vibrational properties of the two PANI forms, we present in Figure 3 the Fourier transform infrared spectra (FTIR) obtained experimentally and theoretically. All the vibration frequencies and their assignments summarized in Table 2 were obtained by referring to the literature [8,18,19]. Experimental spectra are normalized by referring to the band localized at 1124 cm^{-1}, which corresponds to the benzenoid ring vibration.

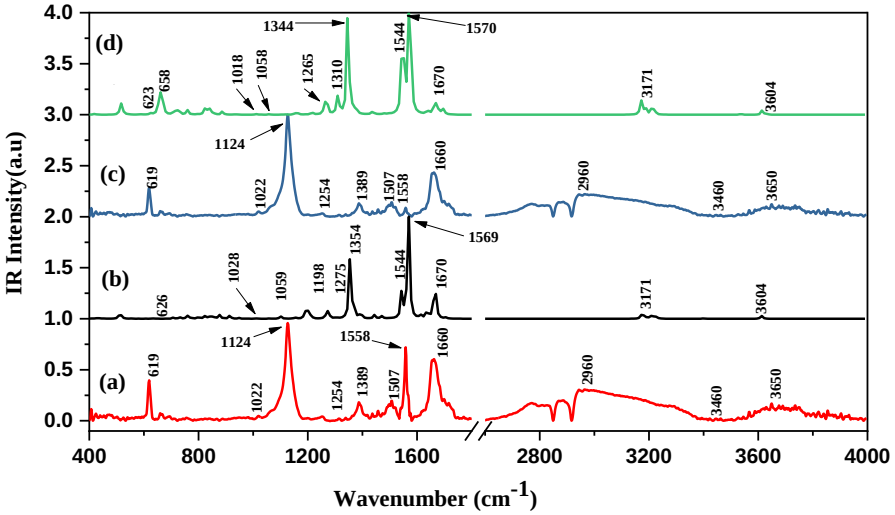

Figure 3 FTIR Spectrum of PANI-EB (a) : experimental, (b) : theoretical and Leucomeraldine (c) : experimental, (d) : theoretical.

Table 2 Positions and Assignments of FTIR absorption band of polyaniline.

Leucomeraldine		Emeraldine base		Assignment
$\upsilon_{Exp.}$ (cm^{-1})	$\upsilon_{Th.}$ (cm^{-1})	$\upsilon_{Exp.}$ (cm^{-1})	$\upsilon_{Th.}$ (cm^{-1})	
619	658	619	626	C-N Deformation
1022	1028	1022	1030	CH Deformation
1124	1058	1124	1059	Ring vibration
1254	1265	1254	1275	C-N (ring) stretching
1389	1354	1389	1346	CH twisting
1501	1544	1501	1544	Ring deformation
1558	1570	1558	1569	C=N and C=C (ring) twisting
1660	1670	1660	1670	aromatic deformation
2960	3171	2960	3171	symmetric CH vibration
3460	--------	3460	------	Asymmetric CH vibration
3650	3604	3650	3604	N-H vibration

Compared to the experimental spectra, all the bands are found within the theoretical spectra with a relatively systematic shift. This deviation from experimental frequency is due to the fact that theoretical calculations are done on isolated molecules in gaseous phases, whereas the experimental spectra have been obtained in the solid state. Therefore, interchain interactions are not considered. Moreover, while the real chain is a polymer, theoretical calculations consider a modeling structure of only 4-units. The peak at 619 cm^{-1} corresponding to the C-N deformation in the plane [8] is found theoretically at 658 cm^{-1} and 626 cm^{-1}, respectively, for leucoemeraldine and emeraldine bases. With the same intensity, the band located at 1022 cm^{-1} attributed to the C-H deformation in the plane is also theoretically present at 1028 and 1030 cm^{-1}, respectively, for both materials. Peaks at 1124 cm^{-1} and at 1501 cm^{-1} are associated with ring deformation and are also found in the theoretical spectrum at 1058 cm^{-1} and at 1544 cm^{-1}, respectively. While peaks at 1254 cm^{-1} and at 1389 cm^{-1}, assigned to C-N vibrations and in the plane CH switching, appear with relatively high intensity at on theoretical spectra at the frequencies of 1265 cm^{-1} and 1344 cm^{-1}.

The presence of a 1558 cm^{-1} band, attributed to the quinoidal C=C stretching [19] with respectively low (high)

intensity in the case of leucoemeraldine (emeraldine base), can be explained by the fact that the amount of the added acid can achieve this transformation. For the case of PVK (Table 3), our calculations were compared with the experimental study of PVK reported in our previous study. [9]. Theoretical and experimental spectra (figure 4) show a good similarity in terms of band intensity and positions with a shift of a maximum few tens of cm^{-1}.

Experimentally, the two insensitive bands at 717 and 742 cm^{-1} are considered characteristic of carbazole groups, and we assigned them the C-H deformation and C-H swing, respectively. On the other hand, the two bands situated at 1450 and 1481 cm^{-1} with medium intensity are attributed respectively to the aromatic ring vibration of the vinyl carbazole and CH2 tilting. However, the bands at 1156 and 1220 cm^{-1}, with weak intensities, are considered modes of vibration assigned to the in-plane aromatic CH deformation and the C-N vibration, respectively. Also, we note a mean vibration at 1324 cm^{-1} attributed to the CH shift of the vinyl group, as indicated in the literature [9]. As shown in Table 4, the other low-intensity peaks located respectively at 418, 615, 921, 1001, 1024, 1402, 1596, 1624, and 2970 cm^{-1} correspond respectively to the vibrations and deformations of the benzene ring, deformation core, and core C-C vibration, C-C stretching and tilting, CH2 deformation of the vinylidene groups, VK aromatic ring vibration, CH2 tilting, CC and C = C stretch in the benzene ring, aliphatic CH stretching and antisymmetric CH-CH2 stretching [9].

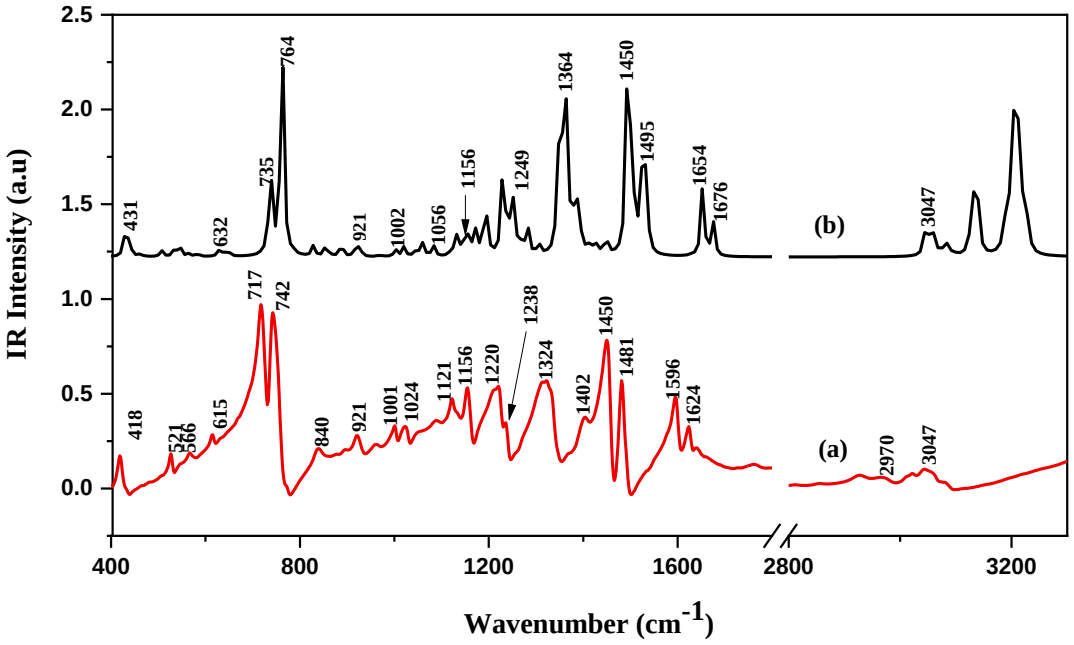

Figure 4 FTIR Spectrum of PVK (a): experimental, (b): theoretical.

Table 3 Positions and Assignments of FTIR absorption band of poly(vinyl carbazole).

$\upsilon_{Exp.}$ (cm^{-1})	$\upsilon_{Th.}$ (cm^{-1})	Assignment
418	431	Benzene ring vibration
615	632	Benzene ring deformation
717	735	CH deformation
742	764	CH twisting
921	925	Aromatic C-C vibration
1001	1002	Aliphatic C-C twisting
1024	1056	C-C vibration
1156	1156	In the plane, aromatic CH deformation
1220	1249	C-N Vibration
1324	1364	CH twisting vinyl groups
1402	1450	Vinylidene CH2 deformation
1450	1495	VK aromatic cycle Vibration
1596	1624	Aromatic C-C and C=C stretching

1624	1676	Aromatic C-C stretching
2970	3047	aliphatic C-H stretching

The experimental absorption spectrum of the leucoemeraldine presented in Figure 5-a shows three optical transitions centered at 217 nm, 249 nm, and 284 nm, respectively. The first two transitions are respectively attributed to σ - σ * and σ - π / π - σ * [20]. The third transition is, however, ascribed to the π - π * , where its extrapolation at the onset of absorption can give the band gap [21]. As shown in the theoretical spectra, these transitions are found at 189, 228, and 294 nm, respectively, demonstrating a good correlation between our experimental and theoretical results, which supports the choice of the modeling structure. For the emeraldine base (Figure 5-b), the spectrum is strongly affected. By referring to the leucomeraldine spectrum, a second spectral range is added in the visible range, starting from 451 nm to 800 nm. As the emeraldine base results from the acid doping process, this new band is, in our opinion, the consequence of the quinoid form, inducing the creation of localized states within the material band-gap [21].

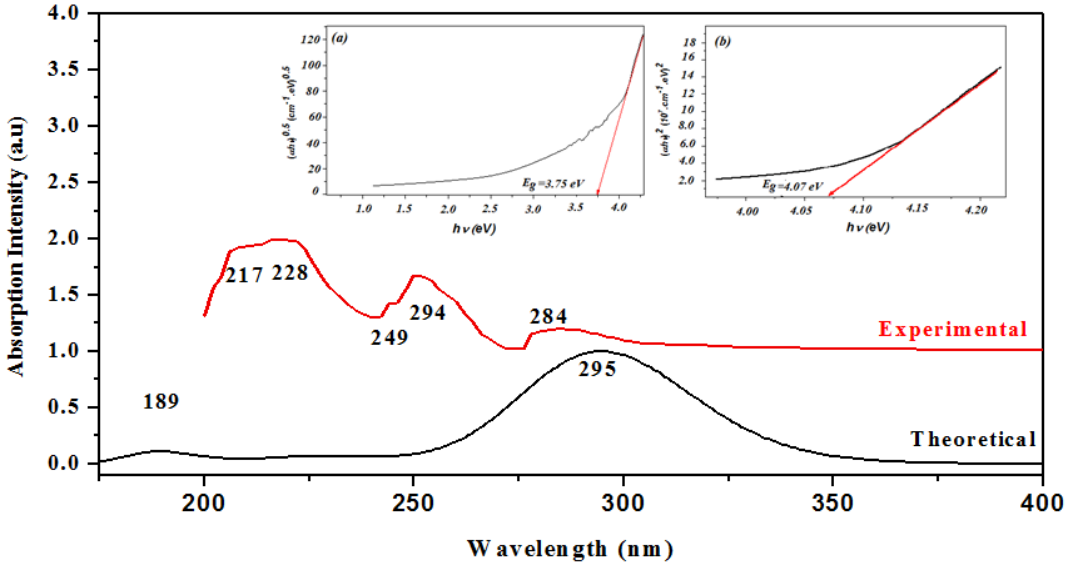

Figure 5-A Experimental and theoretical optical Absorption of Leucomeraldine and Evolution of $(\alpha.h.\upsilon)^{1/m}$ for (a) indirect and (b) direct

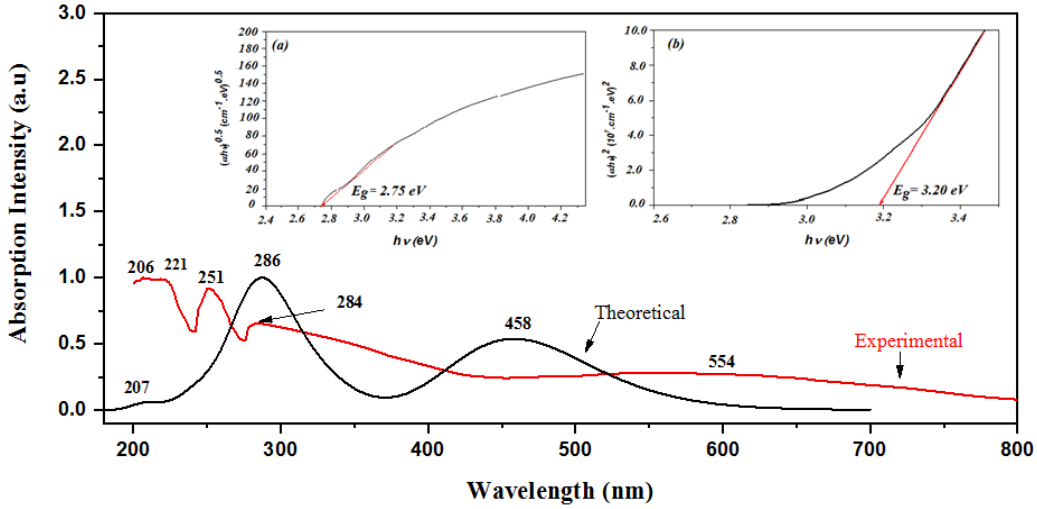

Figure 5-B Experimental and theoretical optical Absorption of Emeraldine Base and Evolution of $(\alpha.h.\upsilon)^{1/m}$ for (a) indirect and (b) direct transition.

To argue the above-presented characteristics of the two forms of polyaniline, we proceeded to the calculation of the absorption spectrum using the DFT method. The theoretical spectra show the presence of the same band cantered at λmax= 458 nm, giving rise to a threshold energy of 2.17 eV. We conclude then that the created band is the consequence of the quinoidal form imposed by the doping process.

By referring to the literature, the PVK/PANI composite, including synthesis and characterization, has not yet been studied. Therefore, we will try theoretically to select the most appropriate form (from both materials) which can lead to a stable composite based on the optical and electronic properties. In Figure 6, we present the optical absorption spectra of PVK, in which there is good accordance between the experimental and theoretical data. Five absorption bands are identified respectively at 231, 263, 295, 332, and 343 nm, as previously reported by Ouro Djobo et al. [22], proving its transparency in the visible range and classing it as a good absorber in the near visible UV spectral domain.

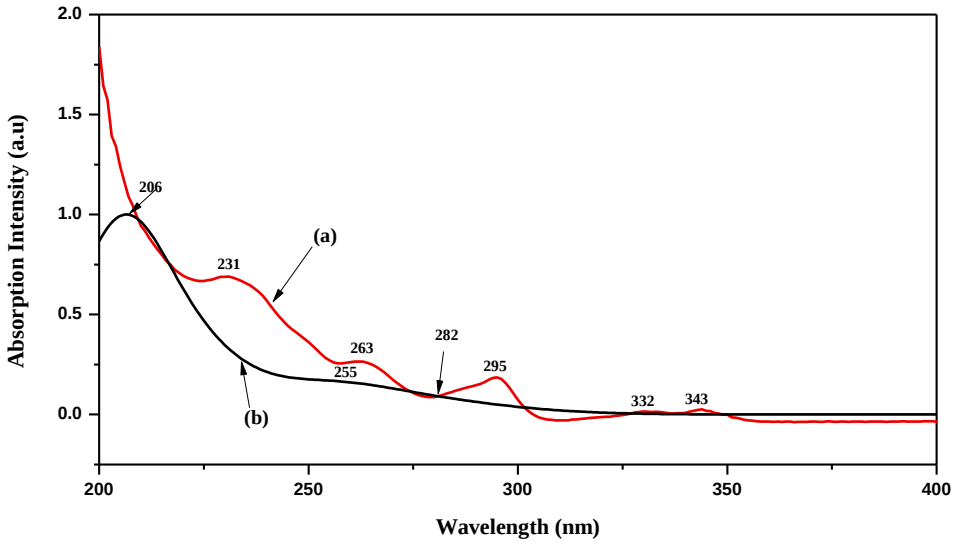

Figure 6 Optical Absorption of PVK: experimental, (b): theoretical.

To make results easier to read, we present in Table 4 the most weighted electronic transitions of either PANI (emeraldine base or leucomeraldine) and those of PVK. For the PVK polymer, three possible transitions are present. The first is associated with the HOMO → LUMO transition and corresponds to the energy of 4.39 eV. The second transition relative to HOMO-3 → LUMO is situated at λmax= 179 nm (4.85 eV). The third transition corresponds to the transition HOMO → LUMO + 3 at 206 nm (6.01 eV).

In order to evidence the nature of these transitions direct (indirect), the Tauc relation [23] can be used. Independently of the crystalline or amorphous materials, this relation relies on the absorption coefficient (α), the optical gap (Eg), and the incident energy h.υ (Equation 1) [23]

$$(\alpha.h.\upsilon) = B.(h\upsilon - Eg)^{m} \quad (1)$$

In this equation, m is a coefficient taken equal to 0.5 for indirect transitions and 2 for direct transitions. Thus, the representation of $(\alpha.\ h.\ \upsilon)^{1/m}$ as a function of hυ makes it possible to evidence the value of the direct and indirect gap [23]. Experimentally, the absorption coefficient is determined by the formula:

$$\alpha = (2.303\ A)/T \quad (2)$$

Where A is the absorbance, and T is the sample thickness estimated by the consideration of both its surface (on the top of silica substrate) and its density. As shown in the onset of Figure 5-a, the evolution of $(\alpha.h.\upsilon)^{1/m}$ versus hυ for leucoemeraldine gives an indirect (direct) gap of 3.75 eV (4.07 eV). The linearity in both cases demonstrates the absorption process in the Leucoemeraldine is dominated by both direct and indirect transitions. The same study in the case of the emeraldine base gives values of 2.75 eV and 3.20 eV, respectively, for indirect and direct transitions. This optical gap decrease is the signature of a localized state creation within the band gap. It is to be noted that the absence of a linear part on the absorption edge for the

emeraldine base for indirect transition indicates that only direct transition contributes to the absorption process.

Table 4 Electronic transition, wavelength and oscillator strength of Polyaniline and PVK.

Materials	Transition	λ (nm), E (eV)	λ_{Th} (nm), E (eV)	f (md/Å)	Assignment (percentage)
Emeraldine base	S0 → S1	284 (4.36)	294 (4.24)	0.7494	HOMO→LUMO (+21%) HOMO→ LUMO+1 (+53%)
	S0 → S2	249 (4.97)	228 (5.40)	0.1042	HOMO-2→ LUMO (+18%) HOMO→ LUMO+6 (+34%) HOMO-1→ LUMO+5 (29%)
	S0 → S3	217 (5.17)	189 (6.57)	0.1086	HOMO-1→ LUMO+5(+21%)
Leucomeraldine	S0 →S1	554 (2.23)	458 (2.71)	0.6797	HOMO→ LUMO (+67%) HOMO-1→ LUMO (+20%)
	S0 → S2	284 (4.36)	286 (4.34)	0.0265	HOMO→ LUMO+2 (+65%)
PVK	S0→ S1	282.7 (4.39)	295 (4.2)	0.1256	HOMO → LUMO (40%) HOMO– 1 → LUMO + 1 (28%)
	S0→ S2	255.6 (4.85)	263 (4.71)	0.1256	HOMO – 3 → LUMO (+39%) HOMO– 2 → LUMO +1(+34%) HOMO → LUMO+3 (+18%)
	S0→ S3	206.0 (6.01)	----------	0.0405	HOMO → LUMO+3(+20%)

The skin depth incident energy, represented in Figure 7, is another optical parameter that can differentiate between the two PANI forms. It is defined as the length traveled by a wave before a coefficient attenuation equal to 1/ e, given by the formula [23]:

$$\boldsymbol{\delta = 1/\alpha} \quad (3)$$

In the case of the emeraldine base, the skin depth presents a maximum value of 0.0288 cm for energy equal to 1.13 eV and then decreases exponentially until reaching cut-off energy equal to 1.8 eV. However, in the case of leucoemeraldine, the skin depth at the energy of 1.13 eV, which is nearly at 0.0251 cm, shows a progressive monotonic decrease until reaching its cut-off energy of 4.82 eV. This shows that in the corresponding absorption spectral region, both materials can drive an incident beam over thickness layers in the order of microns. It is to be noted that the skin depth is much wider in the case of leucoemeraldine compared to that of the emeraldine base due to the narrowing of the transparency region imposed by the creation of electronic transitions within the optical gap. For the PVK, we note that the skin depth is maximized at 0.255 cm for an energy of 3.44 eV, and its corresponding cut-off energy is nearly 4.11 eV. It should be noted that, by referring to both PANI forms, the PVK presents a skin depth ten times higher, proving that PVK in this spectral range can be used as a wave transmission window.

The optical gap decreases, and the skin depth variation, by referring to the emeraldine base, permits us to conclude that localized states are created within the optical band gap. The description of localized states, as well as their energetic width, can be obtained by referring to Urbach's law defined by equation 4 [24]:

$$\boldsymbol{\alpha = \alpha_0 . \exp\left(h.\nu / E_U\right)} \quad (4)$$

Where hυ is the incident radiation, Eu is the Urbach energy often interpreted as the width of the band of localized states. Equation 2 can also be rearranged as follows (Equation 5).

$$\boldsymbol{ln(\alpha) = ln(\alpha_0) + (h.\nu)/E_U} \quad (5)$$

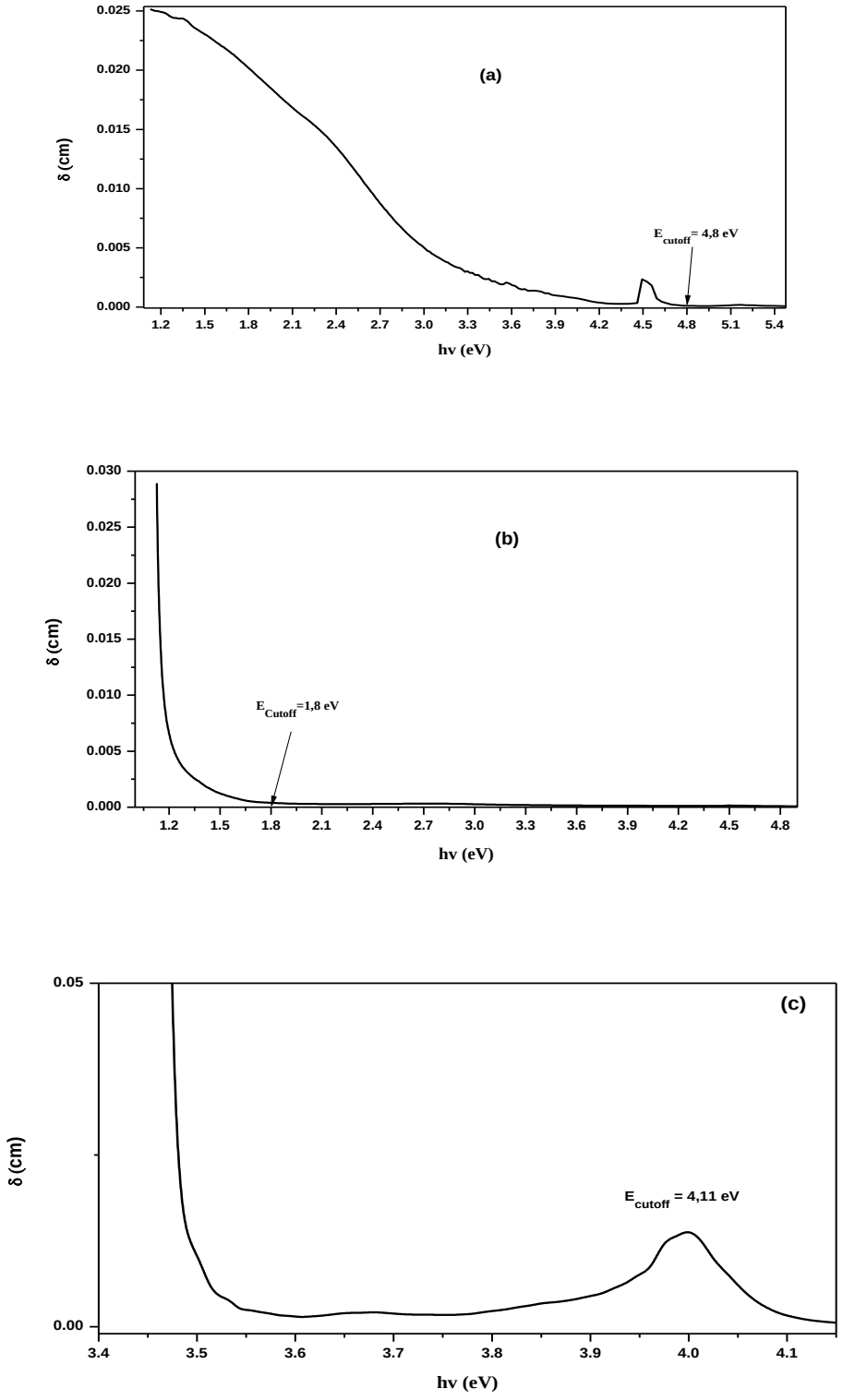

Figure 7 Skin depth of (a) Leucomeraldine and (b) Emeraldine Base and (c) PVK.

In fact, localized states can be generated only in the case of a doped process, which corresponds to the emeraldine base. In Figure 8, we present the evolution of ln (α) as a function of (hυ) in the case of emeraldine base. From the obtained slope in the linear part, a bandwidth Eu equal to 191.3 meV is obtained.

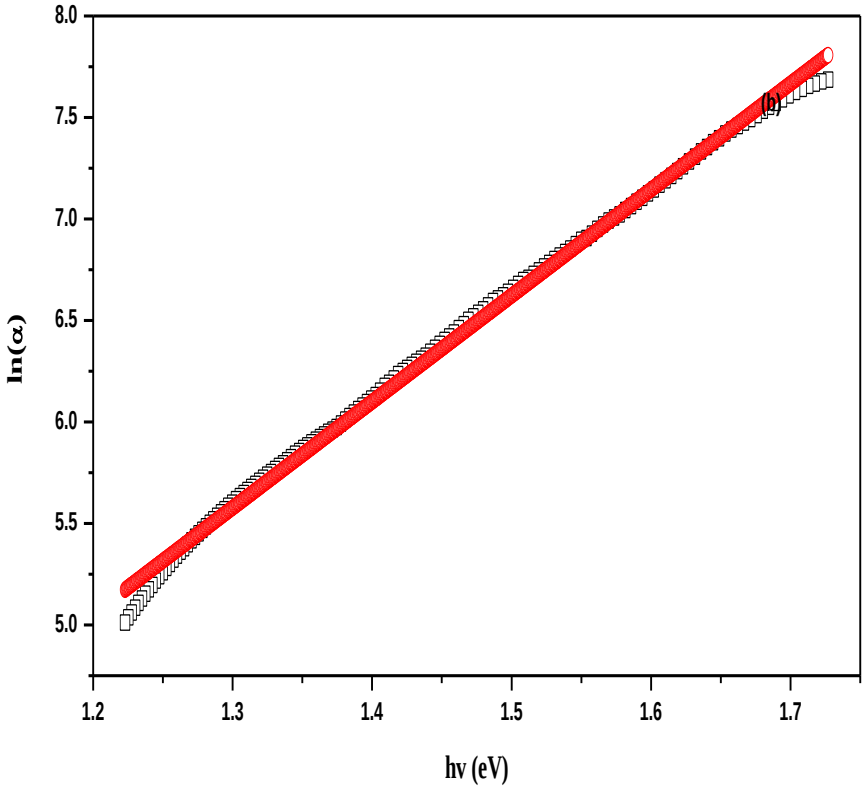

Figure 8 Plot of Ln (α) versus hυ (□), and linear fit (○).

To evidence donor and acceptor character, it will be of interest to carry out HOMO and LUMO levels and their corresponding H - x, and L + x (x, integer x ≻ 0) [25]. These values are useful to support the properties of internal contact or external electrodes, which require certain conditions of compatibility [26]. Thus, the computational study carried out on the leucoemeraldine, emeraldine base structures, as well as PVK makes it possible to elucidate the electronic structures represented in Figure 9. According to the obtained values, we see that the leucomeraldine form has nearly the same electronic band gap, and their corresponding HOMO and LUMO levels present good compatibility with those of PVK by comparison to the emeraldine base. Therefore, the resulting interpenetrating network will be more effective when choosing emeraldine and PVK as hybrid organic materials for both reasons. First, PVK and EB compounds lead to a more broader spectrum and, therefore, more compatibility with the solar spectrum. The second is the donor character from VK to the EB moieties, which can be exploited in the amelioration of power conversion efficiency.

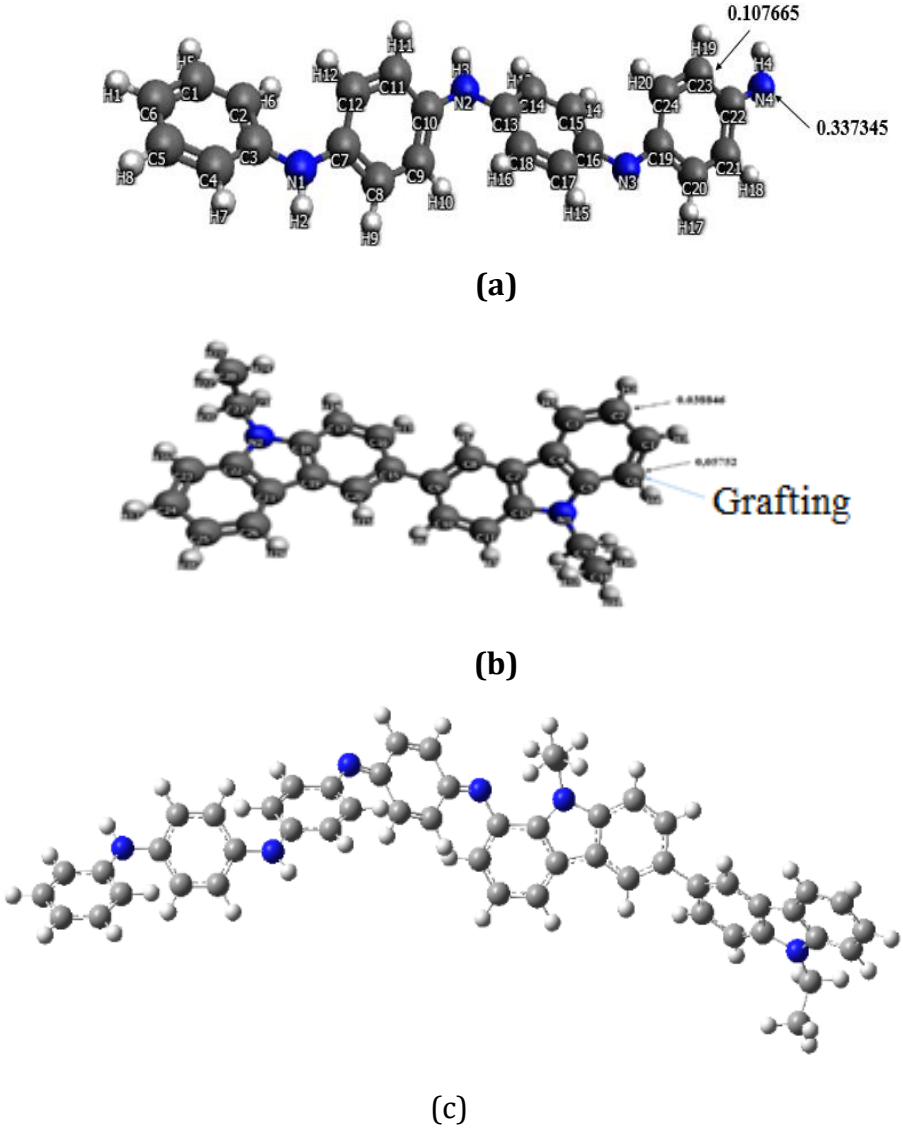

Figure 9 Spin density of (a) PANI-EB and (b) PVK cross linked (c): theoretical calculated structure of the nano-composite PANI-EB / PVK.

By combining experimental and theoretical studies, it has been demonstrated that the easier doping process is an effective tool to modulate the leucoemeraldine properties. Mainly, we noted the energy gap decrease accompanied by the creation of localized states that are placed in the band gap of the material. These changes are confirmed by theoretical calculations, which are closely in good agreement with the experimental results. It has been demonstrated from the electronic structures that only EB can be functionalized with PVK to form an effective Donor/Acceptor hybrid material, presenting good compatibility with the solar spectrum.

To evidence the properties of the resulting PANI-EB/PVK/SWCNTs nano-composites, it is firstly important to carry out the interaction nature between PVK and PANI-EB based on their most interactive sites. The experimental procedure is similar to the already published in the case PPV/PVK [27], where PVK is placed in the presence of (FeCl3) as an oxidant in the (CHCl3) solution. The oxidation of PVK contributes to the formation of polymeric units of vinylcarbazole by the "cross-linking" of VK monomer, as shown in Figure 9. This protocol is justified by spin density theoretical calculations carried out on either carbazole or

PANI units in their oxidized forms (Figures 9-a and 9-b). Our Calculations show that the high spin density is localized in the azote atom of PANI and the carbon atom (1, 8) of the PVK sequence. Then, we concluded that the azote atom of PANI units would be grafted onto the equivalent carbon atoms numbered (1, 8) of PVK (Figure 9-c)

The calculation carried out on this structure gives the optimized structure shown in Figure 9-c, with a stabilization energy of Estab = -2335.371 Ha. The determination of electronic parameters such as gap energy (Eg), electronic affinity (AE), and ionization potential (PI), presented in Figure 10, makes it possible to know the process of local charge transfer between both components.

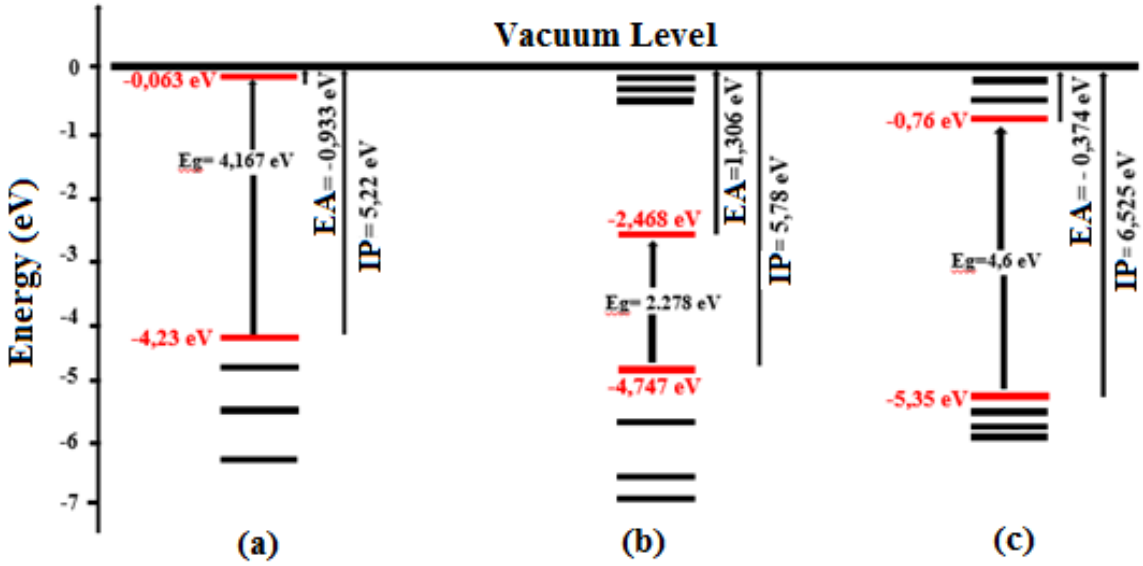

Figure 10 Electronic structure of: (a) leucomeraldine, (b) emeraldine base and (c) PVK.

Based on the theoretical absorption spectra presented in Figure 11, the PANI/PVK shows a browed band ranging from 400 to 800 nm and centered at λmax= 540 nm. This significant red shifting is associated with the localized states in the visible range. Due to better compatibility with the solar spectrum, allowing it to exploit all wavelengths below 800 nm, the PANI/PVK composite is a promising candidate for photovoltaic applications. From the electronic structure of Figure 11-b and by referring to the PANBI-EB, the LUMO of the composite (PANI—EB/PVK) has been reduced by 0.162 eV, while its HOMO has been increased by a quantity of 0.117 eV, allowing a gap reduction by 0.28 eV. This reduction is associated with the increase in the conjugation length of the PANI-EB/PVK chains [28].

The carbon nanotube used to be functionalized with the resulting compound has been shown to have a lower radius (0.72 nm) to give a better dispersion process and to have more nano-junctions. In our case, we are limited to the armchair tube with chirality indices n = m = 5. The perfectly optimized structures with a stabilization energy Estab = -4966.249 Ha are shown in Figure 12. Theoretical calculations give HOMO and LUMO energy levels and a band gap (Eg) of respectively -4.30 eV, -2.93 eV and 1.37 eV. Moreover, the isosurface analysis of the corresponding molecular orbitals provides a reasonable indication of interesting electronic properties and charge transport. Indeed, we have mapped the isosurfaces of the SWCNTs (5.5) molecular orbital contours, as shown in Figure 12.

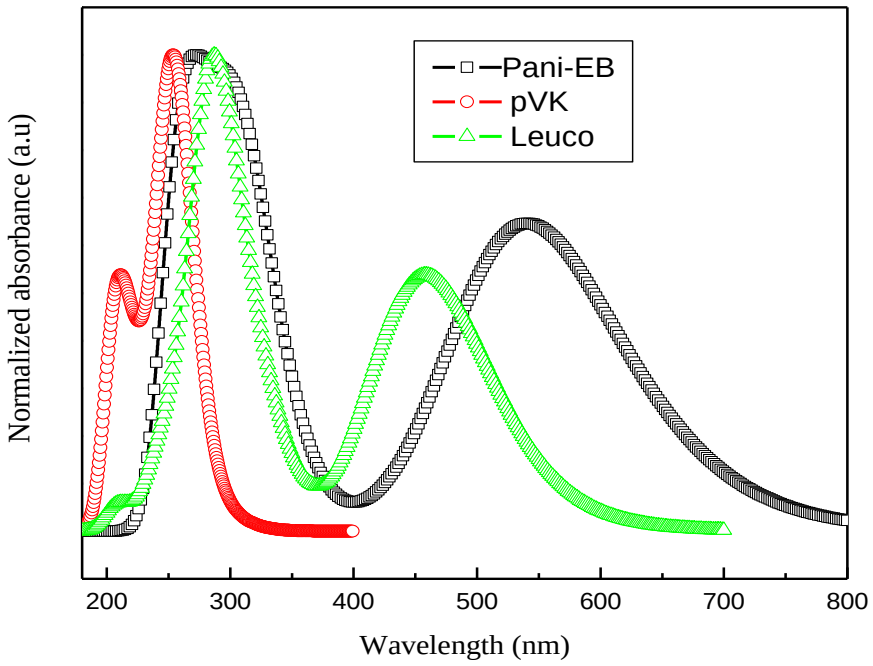

(a)

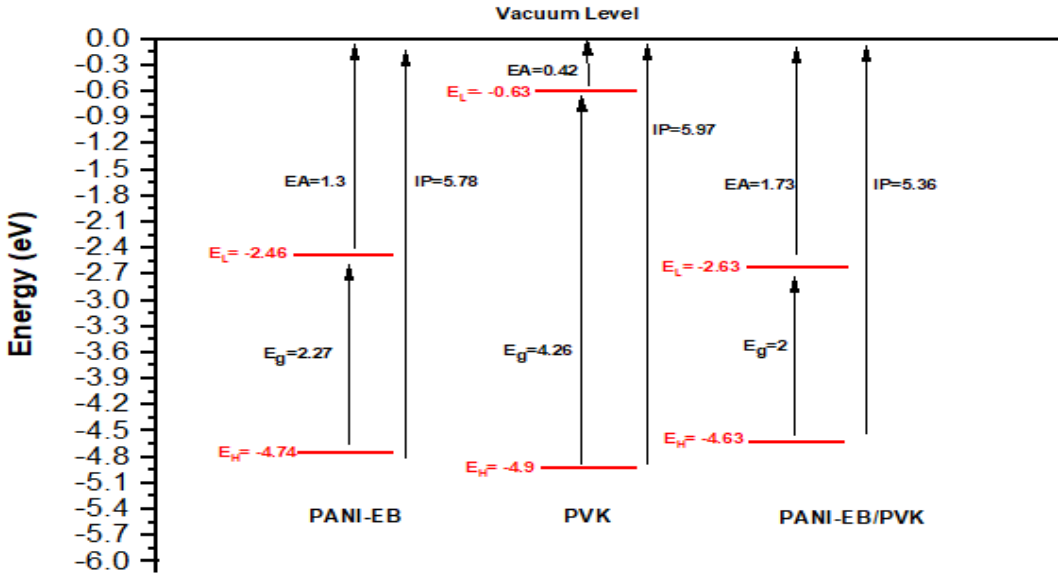

(b)

Figure 11(a) Theoretical optical absorption and (b) electronic structure of the PANI-EB, PVK and PANI-EB / PVK composite.

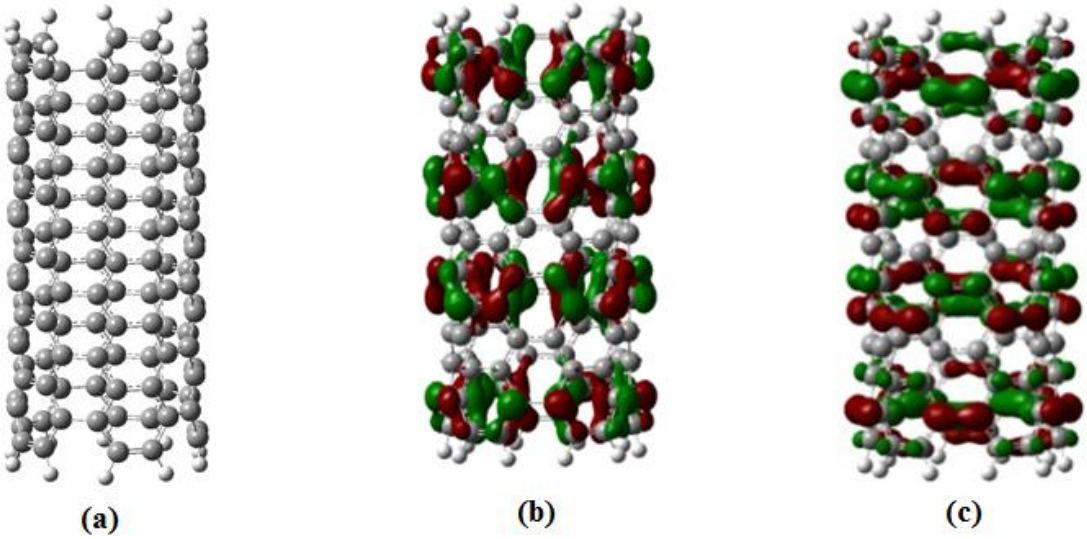

Figure 12 Perfectly optimized structure (a) and representation of the contours of molecular orbitals HOMO (b), LUMO(c) of SWNTC (5.5)

Therefore, compatibility with the solar spectrum allows for absorbance in the large UV, visible, and near-infrared spectral ranges, as suggested experimentally in some cases [29-30].

Frontier molecular orbitals (FMOs) are helpful, namely, those involving the most probable optical transition. In fact, the conductive nature of the material is strictly related to the energy gap [31], defined as the difference between the highest occupied molecular orbital (HOMO) and the lowest unoccupied molecular orbital (LUMO). The charge transfer at the nano-junction imposes a separation process. At the interface PANI-EB/PVK/SWCNTs, electrons that are excited in the hybrid polymer will be transferred in SWCNTs LUMO, and the polymer HOMOs will act as holes. From Figure 12, it can clearly be seen that FMOs of LUMO energies are wrapped in the radial direction. However, those of HOMO are spread over the axial direction of SWCNTs. Because charge mobility is higher in the racial direction, the nano-junction leads to a better conductive property [32]. Then, HOMO or LUMO orbitals are delocalized over the entire molecular skeleton, supporting that there is great spatial overlapping between the HOMO and LUMO. Then, for SWCNTs, the configuration may lead to a strong HOMO-LUMO optical absorption transition [33].

Figure 13 shows the perfectly optimized structure of the PANI/PVK/SWCNTs composite, which has been obtained at the stabilization energy of Estab= -7261.237 Ha.

It is demonstrated that PVK moieties are oriented to cover SWCNTs. The hydrophilic character of the obtained compounds leads to the stabilization and the improvement of the adsorption process. However, due to the hydrophobic character, the PANI is wrapped around the SWCNTs, assuring noncovalent functionalization (type π-stacking). The polymeric configuration of PANI-EB/PVK exhibits a good organization with SWCNTs, resulting in a good (π-stacking) orbital recovery. The resulting structure, with the inter-plane distance, favors the charge transfer between PANI and SWCNTs nanoparticles. These planes that form a particular growth are weakly linked together by Van der Waals forces (inter-plane distance: 4.5 Å). When examining Figure 13-b, it can be noted that the ground state interaction between the PANI-EB/PVK compounds and SWCNTs induces intra-spatial charge transfer states in the resulting composite. This charge transfer takes place mainly between the SWCNTs and the conjugated sequences of PANI-EB. The PVK blocks are, however, grafted onto the wall ends, favoring mechanical enhancement of the global structure.

In Figure 14-a, we propose the architecture of the bulk hetero nano-junction (BHNJ) as an alternative to investigate the power conversion efficiency of organic photovoltaic cells (OSCs). This interconnected network of different layers is currently considered the most widely used for the realization of the CPOs. The organic solar cell consists of the growth of organic layers of a low thickness (typically 100 nm) sandwiched between two metal electrodes. Some parameters are essential for obtaining high-performance solar cells, such as low gap, high oxidation potential, and good charge transport. These parameters govern the values of the open-circuit potential (Voc), the short-circuit current (Jsc), and the form factor (FF), which determine the efficiency (PCE) of a solar cell according to the following equation:

$$\mathbf{P_{CE} = (V_{oc}.\, Jsc.\, FF)/P_{in}} \qquad (6)$$

The relatively low HOMO level of the composite leads to a high value of the open circuit potential (Voc). This potential remains proportional to the energy difference between the HOMO level of the Hybrid polymer and the LUMO level of the SWCNTs (as expressed by Equation 7) and also depends on the work function of the electrodes. In our case, the PANI/PVK has the highest value of around 1.70 eV. The form factor FF, which is a measurement of the ability to generate free charge carriers at the electrodes, is proportional to the high value of the absorption coefficient of the PANI-EB/PVK compound.

$$\mathbf{V_{OC} = 1/e\ (E_{LUMO}\ (SWCNTs) - E_{HOMO}\ (composite)) - 0.3} \qquad (7)$$

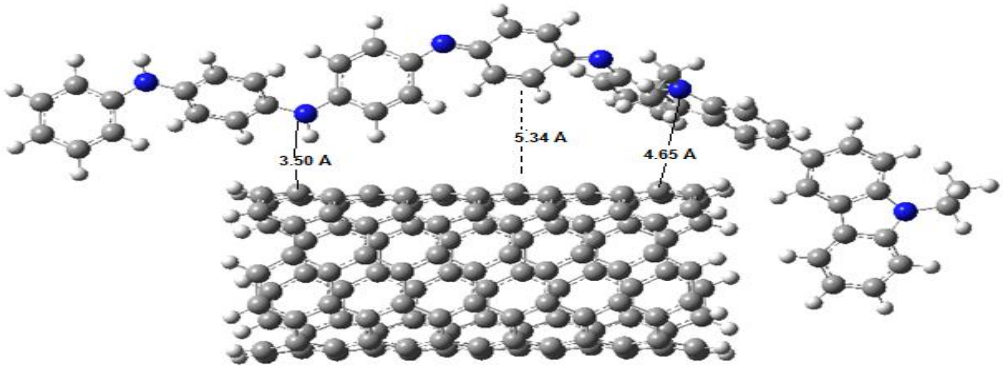

(a)

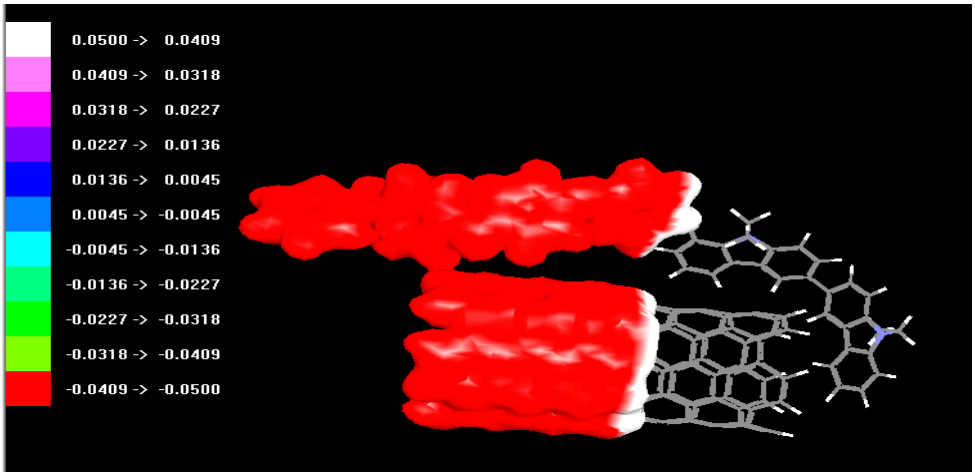

(b)

Figure 13 (a) Optimized structure and (b) potential energy area of PANI-EB/PVK/ SWCNTs (5.5) nano-composite.

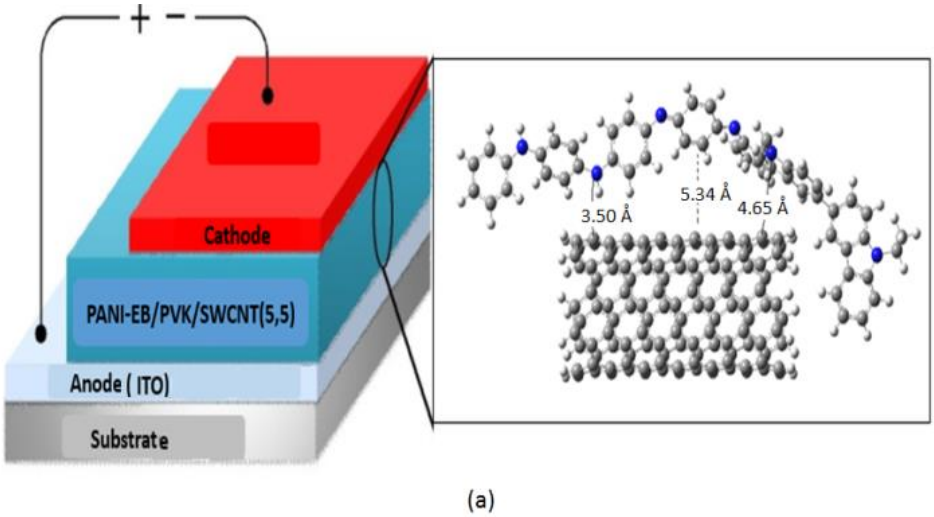

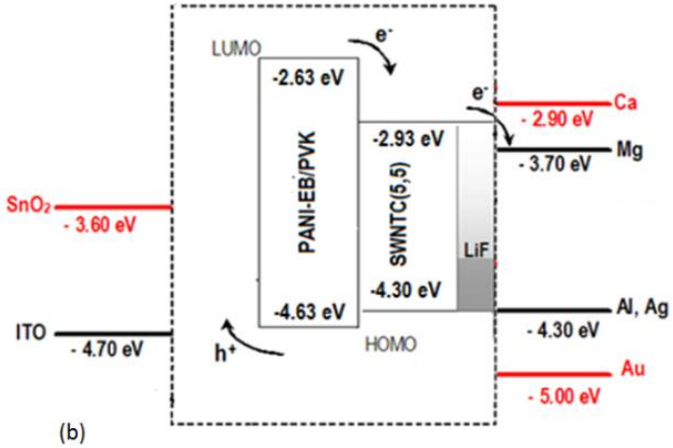

Figure 14 (a) Proposed structure of Bulk Hetero-nano-junction solar cell (BHNJ) based on nano-composite PANI / PVK/SWCNTs (5, 5) and (b) the corresponding Energy diagram

The energy difference (ΔE) between the LUMO level of the PANI-EB/PVK and the LUMO level of the SWCNTs (5.5) is in the order 0.30 eV, leading to an efficient charge transfer [34]. The addition of SWCNTs leads not only to the improvement of photovoltaic performances but also to a better structural organization of the active layer. Qualitatively, the presence of conjugated chains of PANI-EB in the organic composite matrix leads to the improvement of Jsc value due to the intrinsic visible absorption range, which implies better mobility and, consequently, improved photovoltaic efficiency.

In Figure 14-b, we present the energy diagram of the modeling photovoltaic cell. This diagram is composed of the active layer, the Lif layer, and both cathodic and anodic contacts of an ohmic nature. The Lif layer is sandwiched between the cathode and SWCNTs. In order to find compatible electrodes, different metals can be used, such as cathode and anode. It can be noted that ITO and SnO2 as anodes, Calcium (Ca), and Magnesium (Mg) as cathodes are the most suitable for a collection of effective charges on both electrodes. Among them, ITO as anode and Mg as cathode represent the most appropriate choice due to the compatibility of their work functions, respectively, with the LUMO level of SWCNTs and at the HOMO level of the PANI/PVK compound. The presence of a thin layer of LiF between the cathode and the active layer aims to improve the power conversion efficiency of the device by improving its ohmic contact. According to the Sharber et al model [35], and based on the obtained electronic parameters, the PANI-

EB/ PVK/SWNTs power conversion will exceed 7% under optimal conditions. This efficiency value can be further improved by controlling the SWCNTs concentration in the hybrid polymer.

4. CONCLUSION

From the experimental and theoretical study of the two PANI forms, it is found that the Emeraldine base is the most appropriate to form a hybrid PANI/PVK matrix. Then, the photo-physical properties of the PANI-EB/PVK/SWCNTs nano-composite, as well as the design of the organic solar cells with interconnected network layers based on Donor-Acceptor architecture, are described. The incorporation of SWCNTs in the organic matrix PANI/PVK, which represents a challenge in the manufacture of the nano-composite, results from the noncovalent functionalization of SWCNTs with the organic hybrid compound, namely PANI-EB/PVK. This noncovalent functionalization conserves the structure of SWCNTs nanoparticles and preserves their properties. Moreover, this functionalization also leads to the HOMO and LUMO energy levels modulation as well as the resulting band gap and imposes a complex internal charge transfer process (CICT).

REFERENCES

[1] L. L. Zhang, X. S. Zhao, "Chem. Soc. Rev.", 38 (issue 9) (2009) 2520-2531.

[2] R. Abidur, F. Omar, M. H. Md, "Renew. Sust. Energ. Rev.", 161 (2022) 112279.

[3] F. Zhang, K. Yang, G. Liu, Y. Chen, M. Wang, S. Li, R. Li, "Compos. Part A: Appl. Sci. manuf.", 160 (2022) 107051.

[4] C. O. Baker, X. Huang, W. Nelson, R. B. Kaner, "Chem. Soc. Rev.", 46 (issue 5) (2017) 1510-1525.

[5] H. Aydin, B. Gündüz, C. Aydin, "Synth. Met.", 252 (2019) 1-7.

[6] M. Saoudi, B. Zaidi, R. Ajjel, "Polym. Compos.", 40 (Issue S1) (2019) E821-E831.

[7] M. Saoudi, B. Zaidi, A. A. Alotaibi, M. G. Althobaiti, E. M. Alosime, R. Ajjel, "Polym.", 13 (issue 6) (2021) 2595.

[8] M. Saoudi, R. Ajjel, B. Zaidi, "J. Mater. Env. sci.", 7 (2016) 4435-4447.

[9] B. Zaidi, N. Bouzayen, J. Wéry, K. Alimi, "J. Mol. Struct.", 971 (issue 1) (2010) 71-80.

[10] R. Charekhah, Z. Jarrahi, M. Darabi, A. Imani, G. Farzi, "J. Mater. Sci. Mater. Electro.", 30 (issue 1) (2019) 26-36.

[11] P. Schulz, A.-M. Dowgiallo, M. Yang, K. Zhu, J. L. Blackburn, J. J. Berry, "J. Phys. Chem. Lett.", 7 (issue 3) (2016) 418-425.

[12] C. Liu, K. Wang, X. Gong, A. J. Heeger, "Chem. Soc. Rev.", 45 (issue 17) (2016) 4825-4846.

[13] C. Alemán, A. Carlos Ferreira, J. Torras, A. Meneguzzi, M. Canales, A. S. R. Marco, J. Casanovas, "Polym.", 49 (issue 23) (2008) 5169-5176.

[14] F. C. Grozema, D. A. L. Siebbeles, J. M. Warman, S. Seki, S. Tagawa, U. Scherf, "Adv. Mater.", 14 (issue 3) (2002) 228-231.

[15] L. L. Premvardhan, L. P. Lavanya, W.-H. Sebastian, A. P. Linda, J. Y. David, "J. Chem. Phys.", 115 (issue 9) (2001) 4359-4366.

[16] P. R. Sundararajan, "Macromolecules", 13 (issue 3) (1980) 512-517.

[17] T. Mestiri, M. Chemek, J. Rouabeh, K. Alimi, "Comput. Condens. Matter.", 4 (20015) 23-31.

[18] V. S. Jamadade, D. S. Dhawale, C. D. Lokhande, "Synth. Met.", 160 (issue 9) (2010) 955-960.

[19] R. Borah, S. Banerjee, A. Kumar, "Synth. Met.", 197 (2014) 225-232.

[20] W. S. Huang, A. G. MacDiarmid, "Polymer", 34 (issue 9) (1993) 1833-1845.

[21] Y. A. Ismail, F. Mohammad, A. Ahmad, "Macromol. Sci: Part A", 48 (issue 11) (2011) 952-961.

[22] S. O. Djobo, J. C. Bernède, K. Napo, Y. Guellil, "Mater. Chem. Phys.", 77 (issue 2) (2003) 476-483.

[23] A. S. Hassanien, A. A. Akl, "Superlattices Microstruct.", 89 (2016) 153-169.

[24] M. F. Zaki, "J. Phys. Appl. Phys.", 41 (issue 17) (2008) 175404.

[25] Z.-G. Zhang, J. Wang, "J. Mater. Chem.", 22 (issue 10) (2012) 4178-4187.

[26] S. Jung, S. Lee, M. Song, D.-G. Kim, D. S. You, J.-K. Kim, C. S. Kim, T.-M. Kim, K.-H. Kim, J.-J. Kim, J.-W. Kang, "Adv. Energy Mater.", 4 (issue 1) (2014) 1300474.

[27] M. Mbarek, F. Massuyeau, J.-L. Duvail, J. Wery, E. Faulques, K. Alimi, "J. Appl. Polym. Sci.", 130 (issue 4) (2013) pp. 2839-2847.

[28] O. Bouriche, B. Bouzerafa, H. Kouadri, "E-Polym.", 18 (issue 2) (2018) 111–122.

[29] G. Maogang, A. S. Tejas, X. Yu, B. Marco, J. Daniel, A. L. Kyle, J. M. Tobin, C. G. Jeffrey, R. Shenqiang, C. H. Mark, "Nano Lett.", 14 (issue 9) (2014) 5308-5314.

[30] P. Moritz, D. T. Daniel, G. J. Z. Arko, K. Benjamin, S. Flavel, "ACS Omega", 2 (issue 3) (2017) 1163-1171.

[31] H. Sadki, M. Mbarek, B. Bouachrine, M. N. Bennani, J. Wéry, K. Alimi, "Polym. Testing", 66 (2018) 78-86.

[32] J. C. Stallard, W. Tan, F. R. Smail, T. S. Gspann, A. M. Boies, N. A. Fleck, "Extreme Mech. Lett.", 21 (2018) 65-75.

[33] X. Lv, Z. Li, S. Li, G. Luan, D. Liang, S. Tang, R. Jin, "Int. J. Mol. Sci.", 17 (2016) 721-735.

[34] Y. Li, L. Xue, H. Li, Z. Li, B. Xu, S. Wen, and W. Tian, "Macromol. 42 (issue 13) (2009) 4491-4499."

[35] M. C. Scharber, D. Mühlbacher, M. Koppe, P. Denk, C. Waldauf, A. J. Heeger, and C. J. Brabec, "Adv. Mater. 18 (issue 6) (2006) 789-794."

.